JGR Atmospheres

RESEARCH ARTICLE
10.1029/2021JD034855

Quasi-4-Day Wave: Atmospheric Manifestation of the First Symmetric Rossby Normal Mode of Zonal Wavenumber 2

Y. Yamazaki[1], V. Matthias[2], and Y. Miyoshi[3]

[1]GFZ German Research Centre for Geosciences, Potsdam, Germany, [2]Deutsches Zentrum für Luft- und Raumfahrt, Institut für Solar-Terrestrische Physik, Neustrelitz, Germany, [3]Department of Earth and Planetary Sciences, Kyushu University, Fukuoka, Japan

Key Points:

- Climatology of westward-propagating quasi-4-day wave (Q4DW) with zonal wavenumber 2 is presented
- Seasonal amplification is controlled by the critical layer and atmospheric instability
- Arctic sudden stratospheric warmings can lead to an unseasonal enhancement of the wave

Correspondence to:
Y. Yamazaki,
yamazaki@gfz-potsdam.de

Citation:
Yamazaki, Y., Matthias, V., & Miyoshi, Y. (2021). Quasi-4-day wave: Atmospheric manifestation of the first symmetric Rossby normal mode of zonal wavenumber 2. *Journal of Geophysical Research: Atmospheres*, *126*, e2021JD034855. https://doi.org/10.1029/2021JD034855

Received 3 MAR 2021
Accepted 17 JUN 2021

Abstract This paper describes global characteristics of the westward-propagating planetary wave with a period of ~4 days and zonal wavenumber 2, here referred to as quasi-4-day wave (Q4DW), which is considered to be a manifestation of the (2,1) Rossby normal mode. A climatology of the Q4DW is derived from geopotential height measurements by the Aura Microwave Limb Sounder during August 2004–December 2020. In the mesosphere and lower thermosphere (MLT), amplitude maxima occur at mid latitudes in May and August in the Northern Hemisphere, and in February and November in the Southern Hemisphere. With the amplitude exceeding 300 m, the Q4DW sometimes becomes the dominant mode of traveling planetary waves in the MLT. The seasonal variation is largely determined by the zonal mean state. As predicted by previous modeling work, the amplitude grows rapidly with height on the equatorward side of the critical layer, where the zonal mean flow is weakly eastward relative to the wave. The wave growth can be particularly large when there is a region of unstable mean flow across the boundary of the critical layer. This condition is met not only during the seasonal amplification of the Q4DW but also during some Arctic sudden stratospheric warming events, leading to an unseasonal enhancement.

1. Introduction

Classical wave theory utilizes the linearized equations governing atmospheric flow to describe properties of wave motions in the atmosphere (e.g., Lindzen & Chapman, 1969; Forbes, 1995). Under the assumption of a simplified atmosphere without dissipation and zonal mean winds, the linearized equations are separable in latitude and height. The latitude equation is known as Laplace's tidal equation. The solutions to Laplace's tidal equation are expressed in form of Hough functions, which give the latitudinal structure of waves. The height equation specifies the vertical structure of each Hough mode for given atmospheric forcing. In the absence of forcing, the assumption of an isothermal atmosphere with a rigid lower boundary (zero vertical velocity at the surface) leads to a single solution to Laplace's tidal equation. The corresponding Hough functions represent free (unforced) oscillations or normal modes of the atmosphere.

The normal modes consist of Rossby modes, Kelvin modes, gravity modes, and mixed Rossby-gravity modes. For an isothermal atmosphere with a temperature, say, $T = 256$K for the Earth, there is a series of westward-propagating Rossby normal modes that have a period longer than a day and shorter than several weeks (Kasahara, 1976; Madden, 2007; Sakazaki & Hamilton, 2020; Salby, 1984). These Rossby normal modes are thought to be responsible for, at least part of, multi-day oscillations commonly seen in atmospheric parameters. An individual Rossby normal mode is often expressed as $(s, n - s)$, where s is the zonal wavenumber and n is the meridional index. The oscillation is symmetric about the equator for an odd number of $n - s$ (=1, 3, 5, ...) and antisymmetric for an even number of $n - s$ (=2, 4, 6, ...). For example (2,1) represents the first symmetric mode $n - s = 1$ with zonal wavenumber $s = 2$, and (1,2) represents the first asymmetric mode $n - s = 2$ with zonal wavenumber 1. The predicted periods of Rossby normal modes include ~4 days for the (2,1) mode, ~5 days for the (1,1) mode, ~7 days for the (2,2) mode, ~10 days for the (1,2) mode, ~16 days for the (1,3) mode, ~28 days for the (1,4) mode. The vertical structure of Rossby normal modes is that of a Lamb wave. The phase of the wave is constant with height. Although the energy decreases exponentially in the vertical, the amplitude grows with height due to the reduction of the density.

In the presence of dissipation and nonuniform background fields, the phase is no longer constant with height, showing vertical propagation characteristics (Salby, 1981a; Salby, 1981b). Also, spectra of Rossby normal modes are suppressed, broadened, and shifted from those predicted by the classical theory (Kasahara, 1980; Salby, 1981b; Salby & Roper, 1980). Nonetheless, normal-mode-like oscillations, or quasi-normal modes, can exist in a realistic atmosphere with latitudinal structures and periods similar to those of classical Rossby normal modes (Salby, 1981a; Salby, 1981b). Salby (1981b) numerically showed that at least (1,1) (1,2) (1,3) (2,1), and (2,2) modes should be detectable as isolated spectral signatures with the expected zonal wavenumbers. In fact, these modes have been widely observed in the lower atmosphere (e.g., Madden, 1979, 2007; Sakazaki & Hamilton, 2020). In the middle atmosphere, the latitude and height structures of Rossby normal modes are strongly influenced by the background atmosphere. Salby (1981a) presented a series of numerical experiments where the (2,1) mode response of the atmosphere is examined under different background conditions. The results that are particularly relevant to the present study are as follows:

1. The vertical growth rate of the wave is reduced in regions where the zonal mean wind is strongly eastward relative to the wave
2. Conversely, the growth rate is enhanced in regions where the zonal mean wind is weakly eastward relative to the wave
3. The wave cannot propagate across the critical layer, within which the zonal mean wind is westward relative to the wave
4. The enhancement and reduction of the growth rate occurs locally without affecting other latitudes, thus introducing a hemispheric asymmetry

As we will show later, the state of the zonal mean atmosphere largely determines the (2,1) mode response in the mesosphere and lower thermosphere (MLT).

Quasi-normal mode oscillations in the middle atmosphere have been studied using global satellite data. Among others, the quasi-6-day wave (Q6DW), which is considered to be a manifestation of the (1,1) mode, is most extensively examined (e.g., Forbes & Zhang, 2017; Hirota & Hirooka, 1984; Qin et al., 2021; Riggin et al., 2006; Wu et al., 1994). Tropospheric processes are thought to be a source of the Q6DW (Miyoshi & Hirooka, 1999). The wave can be amplified or locally excited in the middle atmosphere through an instability of the zonal mean flow (Gan et al., 2018; Lieberman et al., 2003; Liu et al., 2004; Meyer & Forbes, 1997). The Q6DW attains a large amplitude in the lower thermosphere and its influence extends well into the ionosphere (Gu et al., 2014; Yamazaki et al., 2018, 2020). Global features have also been studied for the quasi-10-day wave (Q10DW) and quasi-16-day wave (Q16DW) in the middle atmosphere, which correspond to the (1,2) and (1,3) modes, respectively (e.g., Hirooka, 2000; Hirooka & Hirota, 1985; Day & Mitchell, 2010; McDonald et al., 2011; Forbes & Zhang, 2015). Their sources, sinks, propagation characteristics, and ionospheric effects are still to be established. Only few studies have reported global observations of other normal modes in the middle atmosphere. Zhao et al. (2019) observed a ∼28-day oscillation in the middle atmosphere and associated it with the (1,4) mode. Hirota and Hirooka (1984) showed that westward-propagating ∼4-day oscillations with zonal wavenumber 2 detected in the stratosphere are consistent with the (2,1) mode. Ma et al. (2020) observed westward-propagating ∼4-day oscillations with zonal wavenumber 2 in MLT temperature during the boreal winter in 2018/2019 and associated them with the (2,1) mode. The present study also focuses on westward-propagating ∼4-day oscillations with zonal wavenumber 2 in the middle atmosphere. The oscillations are regarded as a manifestation of the (2,1) Rossby normal mode, and we call them quasi-4-day wave (Q4DW). It is noted that the term "4-day wave" has been sometimes used to designate eastward-propagating ∼4-day oscillations with zonal wavenumber 1 in the polar region (e.g., Allen et al., 1997; Lu et al., 2013; Randel & Lait, 1991). However, they are not a Rossby normal mode, and thus should be distinguished from the Q4DW studied here.

As mentioned earlier, quasi-normal modes in the middle atmosphere are strongly influenced by the zonal mean state of the atmosphere. The implication is that propagation characteristics of quasi-normal modes may be altered when the background atmosphere undergoes significant changes, such as those during sudden stratospheric warmings (SSW) (Andrews et al., 1987; Labitzke & Van Loon, 1999). The response of quasi-normal modes to SSW has been addressed in numerous studies (e.g., Hirooka & Hirota, 1985; He et al., 2020; Matthias et al., 2012; Pancheva et al., 2008; Sassi et al., 2012; Yu et al., 2019; Yamazaki & Matthias, 2019). These studies found that quasi-normal modes are sometimes enhanced around the time of SSW,

but details of the response, such as the period of amplified wave and the timing of amplification relative to the SSW onset, can vary from event to event. The presence of the (2,1) mode has been noted during some SSW. For instance, Sassi et al. (2012) detected the Q4DW during the major SSW in January 2009, but not during other boreal winters (2004/2005, 2005/2006, and 2007/2008). Ma et al. (2020) presented observations of the Q4DW in mesospheric temperature, as well as ~4-day oscillations in zonal and meridional winds at MLT altitudes, during the major SSW in 2018/2019. They suspected that the baroclinic/barotropic instability might be responsible for the amplification of the Q4DW. Baroclinically and barotropically unstable regions arise from large vertical and horizontal shears of the zonal wind, respectively. The unstable regions can provide a source of energy for the enhancement of a wave, and are considered to be important for seasonal and unseasonal enhancements of quasi-normal modes. The role of the baroclinic/barotropic instability has been particularly well studied for the Q6DW (e.g., Liu et al., 2004). The relationship between the baroclinic/barotropic instability and Q4DW activity is yet to be established.

The main objectives of this study are (a) to determine the global seasonal climatology of the Q4DW, (b) to examine the relationship between the seasonal variations of the Q4DW and background atmosphere, and (c) to explore the link between the Q4DW and SSW based on long-term global observations. To this end, we use 16 years of geopotential height and temperature measurements from the Microwave Limb Sounder (MLS) onboard NASA's Aura satellite (Waters et al., 2006). Detailed descriptions of the data and method of the analysis are provided in the following section.

2. Data and Method of Analysis

The primary data employed in this study are geopotential height measurements from Aura/MLS during August 2004–December 2020 (Schwartz et al., 2008; Waters et al., 2006). The data cover the pressure levels from 261 to 0.001 hPa, which correspond roughly to 9 and 97 km, respectively. We use the log-pressure height $z = H\ln\left(p_0 / p\right)$ to approximate the height of the measurements, where H (=7 km) is the scale height, p_0 (=1,013.25 hPa) is the sea level pressure, and p is the pressure. The method for evaluating wave components is the same as that used in Yamazaki and Matthias (2019). The amplitude A and phase ϕ of a wave with zonal wavenumber s and period τ were determined by fitting of the following formula to the data collected at a given latitude and height:

$$\sum_{s=-4}^{4} A_{s,\tau}\cos\left[2\pi\left(\frac{t}{\tau}+s\lambda\right)-\phi_{s,\tau}\right], \tag{1}$$

where t is the universal time, and λ is the longitude. In this definition, s < 0 and s > 0 corresponds respectively to eastward- and westward-propagating waves, and $s = 0$ represents a zonally symmetric oscillation. The least-squares fitting was performed using a time window that is 3 times the wave period and a latitude window of ±5°. Before the fitting, the data were separated into those obtained in the ascending and descending portions of the orbit, and for each group of the data, the mean value was subtracted. The residuals in both groups were used in the fitting. In this way, aliasing from migrating solar tides can be avoided (Meek & Manson, 2009). Signatures of migrating solar tides are stationary in both ascending and descending parts of the orbit, as the Aura spacecraft is in a Sun-synchronous orbit. Signatures of tidal modulation by planetary waves could still alias into the derived signatures of planetary waves because of limited spatial and temporal coverage of the data, but in general, atmospheric perturbations associated with tidal modulation are very small below 100 km (Gan et al., 2017; Miyoshi & Yamazaki, 2020).

Geostrophic winds were derived from the geopotential height measurements using the method described in Matthias and Ern (2018). The zonal mean zonal wind $\overline{u}_g$ was used to identify the critical layer, where the mean flow relative to the wave is westward:

$$\overline{u}_g - C_{s,\tau} < 0. \tag{2}$$

Here $C_{s,\tau}$ is the phase velocity of a wave with zonal wavenumber s and period τ. At latitude ϕ,

$$C_{s,\tau} = -\frac{2\pi a}{s\tau}\cos\phi \tag{3}$$

where a ($= 6.37 \times 10^6$ m) is the Earth's radius.

An instability of the mean flow is evaluated by the potential vorticity gradient, $\overline{q}_y$, defined by

$$\overline{q}_y = \frac{2\Omega}{a}\cos\phi - \frac{1}{a^2}\frac{\partial}{\partial\phi}\left[\frac{1}{\cos\phi}\frac{\partial}{\partial\phi}\left(\overline{u}_g\cos\phi\right)\right] - \frac{1}{\rho}\frac{\partial}{\partial z}\left(\rho\frac{f^2}{N^2}\frac{\partial\overline{u}_g}{\partial z}\right), \quad (4)$$

where Ω ($=7.292 \times 10^{-5}$ rad s^{-1}) is the rotation rate of the Earth, ρ is the atmospheric density, f ($=2\,\Omega\sin\phi$) is the Coriolis frequency, and N is the buoyancy frequency. The density is derived based on the ideal gas law using temperature measurements by Aura/MLS. The buoyancy frequency is derived from Aura/MLS temperature profiles:

$$N^2 = \frac{g}{T}\left(\frac{\partial T}{\partial z} + \frac{g}{c_p}\right), \quad (5)$$

where g is the gravitational acceleration, T is the atmospheric temperature and c_p ($=1004$ JK^{-1} kg^{-1}) is the specific heat of dry air. A necessary condition for the baroclinic/barotropic instability is $\overline{q}_y < 0$. In regions where $\overline{q}_y < 0$, the mean flow is unstable to perturbations, and a wave can amplify by extracting energy from the unstable mean flow.

3. Results and Discussion

3.1. Seasonal Climatology of the Quasi-4-Day Wave

Here we present the seasonal climatology of the Q4DW derived from the long-term record of Aura/MLS geopotential height during August 2004–December 2020. The first two rows of Figure 1 display westward-propagating wave spectra for zonal wavenumber $s = 2$ (W2) and $s = 1$ (W1) at 0.001 hPa (97 km) at mid-latitudes. The W2 component shows a well-defined seasonal pattern in both the Northern and Southern Hemispheres. In the Northern Hemisphere, enhanced W2 wave activity with periods around 4 days are seen in May and August, while in the Southern Hemisphere, similar wave activity is seen in February and November. The results suggest that the Q4DW is the predominant W2 component in the mid-latitude MLT. The mean period of the Q4DW is 3.8 ± 0.4 days, which is close to the predicted period of the (2,1) mode, for example, 3.84 days according to Madden (2007). The spectral peak around 4 days is also observed at other altitudes in the lower thermosphere and upper mesosphere (not shown here). However, in the lower mesosphere and below (say, <65 km), the ~4-day peak is usually not resolved.

The results for the W1 component suggest that the Q6DW is predominant at this height, which is in agreement with previous studies (e.g., Qin et al., 2021). The maximum amplitude of the Q6DW (~250 m) is greater than that of the Q4DW (~180 m). For W1, the period of the dominant wave tends to be shorter during local summer and longer during local winter. This is owing to the fact that the zonal mean zonal wind is more westward during local summer in large part of the middle atmosphere (20–90 km), as shown in the panels in the third row. Since shorter-period waves have larger phase speed, they are more likely to reach higher altitudes without encountering the critical layer during local summer. The period of the dominant W2 wave seems to show a similar seasonal pattern, but the amplitude is small during the local winter, so that it is difficult to determine the period.

The bottom panels of Figure 1 show the meridional structures of the Q4DW and Q6DW at a height of 97 km. The Q4DW amplitude is defined here as the maximum amplitude of W2 waves with a period between 3–5 days. Similarly, the Q6DW amplitude is defined as the maximum amplitude of W1 waves with a period between 4.5–7 days. At 97 km, amplitude maxima occur about ±45° latitudes for both the Q4DW and Q6DW. The mid-latitude maxima in geopotential height perturbations are consistent with the meridional structures of the (2,1) and (1,1) modes, which are indicated by the white dashed curves.

The vertical structure of the climatological mean Q4DW is depicted in Figure 2 for February 11, May 17, August 11, and November 15, when the amplitude is relatively large in the MLT. The gray lines in the figure indicate the boundary of the critical layer. That is, the zonal mean wind relative to the wave is westward in areas poleward of the lines. As mentioned earlier, the Q4DW cannot propagate across the critical layer.

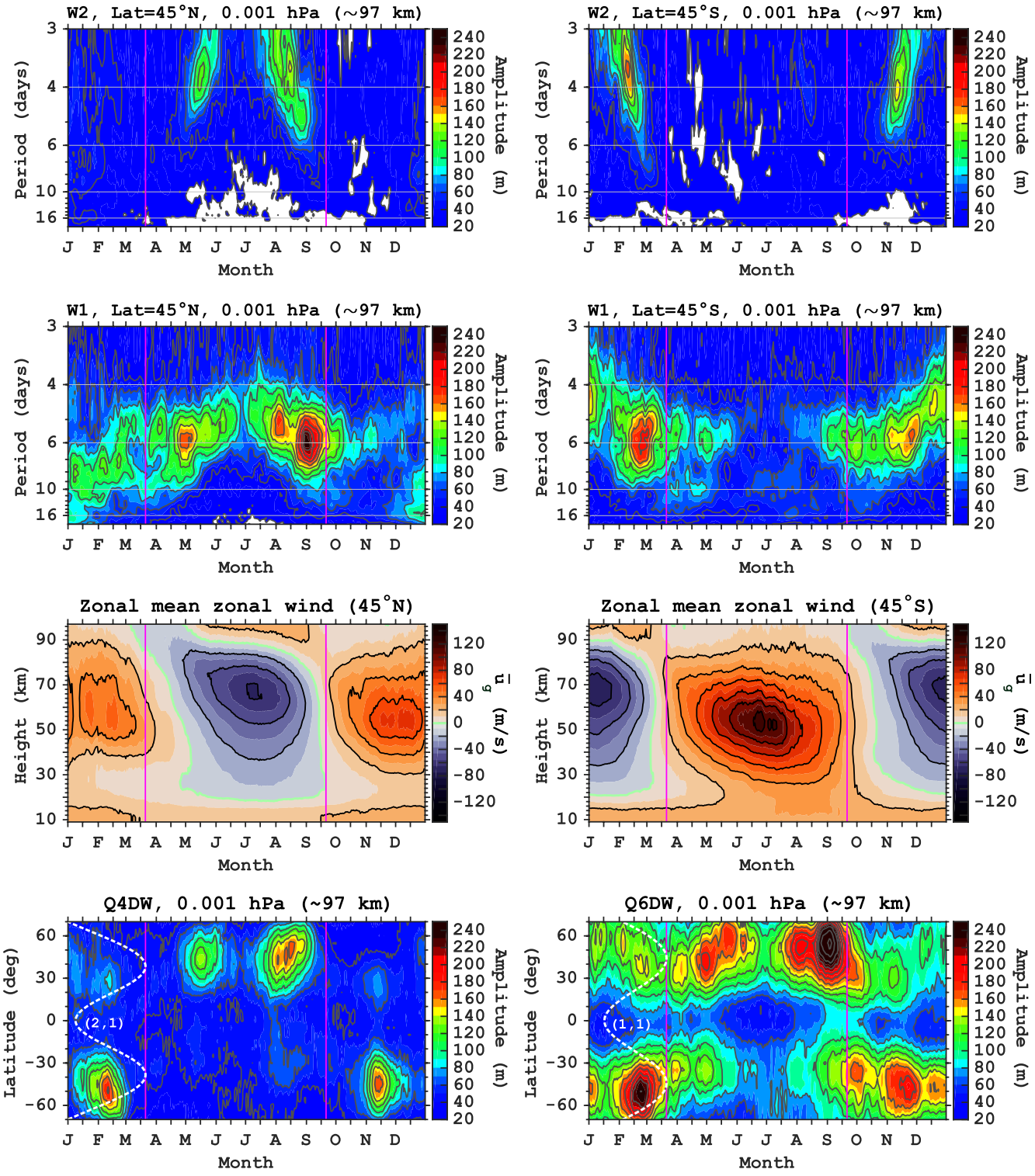
W2, Lat=45°N, 0.001 hPa (~97 km)
W2, Lat=45°S, 0.001 hPa (~97 km)
W1, Lat=45°N, 0.001 hPa (~97 km)
W1, Lat=45°S, 0.001 hPa (~97 km)
Zonal mean zonal wind (45°N)
Zonal mean zonal wind (45°S)
Q4DW, 0.001 hPa (~97 km)
Q6DW, 0.001 hPa (~97 km)
Period (days)
Height (km)
Latitude (deg)
Month
Amplitude (m)
(2,1)
(1,1)

Figure 1

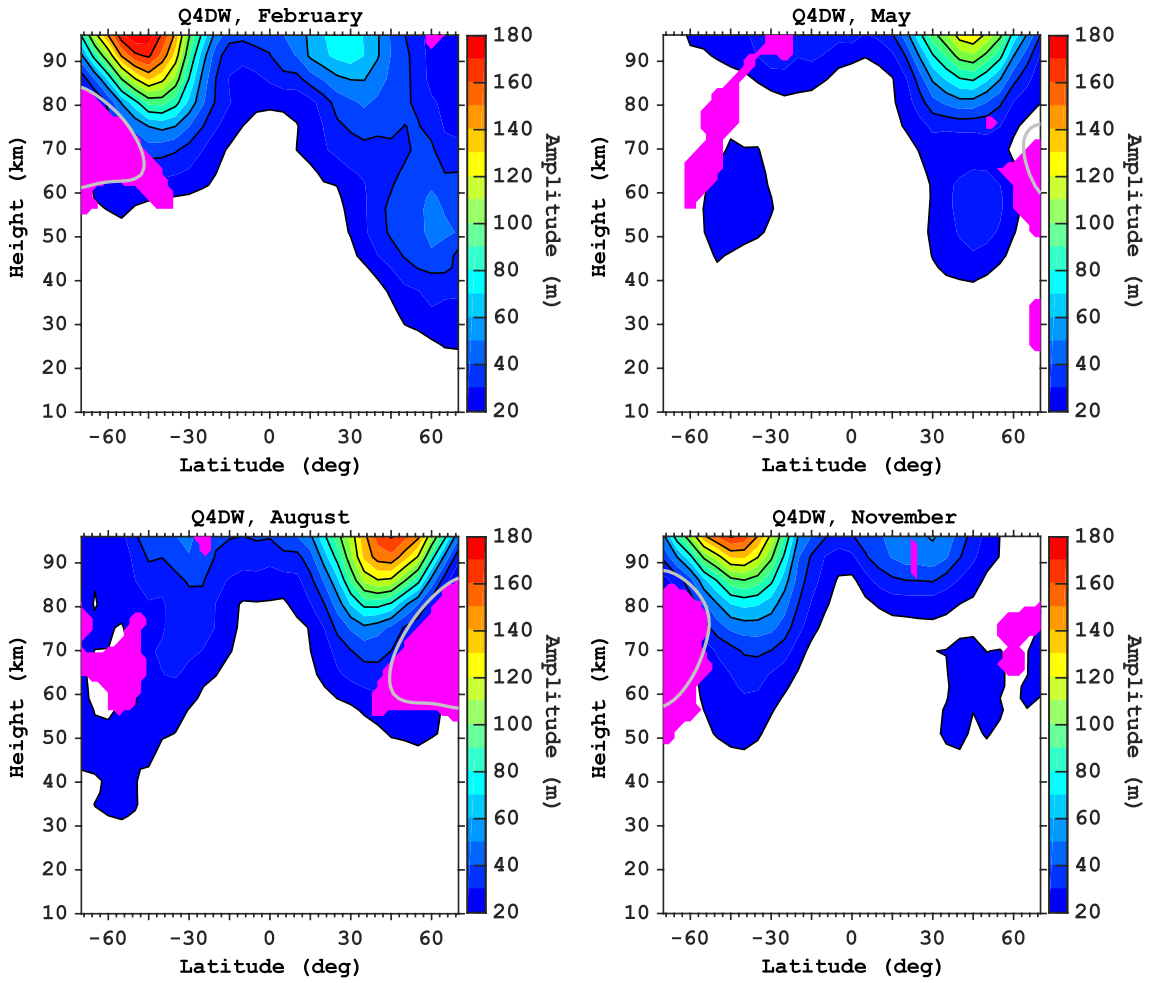

Figure 2. Latitude versus height distributions of the amplitude of the quasi-4-day wave (Q4DW) for 11 February (top left), 17 May (top right), 11 August (bottom left), and 15 November (bottom right). They are climatological representations based on the average of 16 years of the Aura/Microwave Limb Sounder geopotential height observations. The gray lines indicate the boundary of the critical layer for the Q4DW. The magenta shading indicates regions of unstable zonal mean flow ($\overline{q}_y < 0$).

It is seen that the Q4DW grows rapidly in the vertical near the equatorward boundary of the critical layer, which is consistent with the numerical results by Salby (1981a). Magenta colored areas in Figure 2 indicate regions where the necessary condition for the baroclinic/barotropic instability is met, that is, $\overline{q}_y < 0$. In all cases, there is an unstable region around the critical layer, at altitudes of 50–70 km. Thus, it is possible that the Q4DW is amplified or locally excited in the mesopause region.

Figure 3 shows the vertical structure of the climatological mean Q4DW in equinox and solstice conditions, when the amplitude is relatively small. During the equinoxes, unstable regions ($\overline{q}_y < 0$) are seen at high latitudes but there is no critical layer, around which the wave can rapidly grow. During the solstices, a critical layer is seen in the summer hemisphere. However, unlike the times of the seasonal amplification of the

Figure 1. Spectra of Aura/Microwave Limb Sounder (MLS) geopotential height at 0.001 hPa (97 km) during August 2004–December 2020. The top panels show month versus period distributions for the westward-propagating zonal wavenumber 2 (W2) component at 45°N (left) and 45°S (right), while the panels in the second row are for the westward-propagating zonal wavenumber 1 (W1) component. The panels in the third row show the zonal mean zonal wind at 45°N (left) and 45°S (right), as derived from Aura/MLS geostrophic winds. The bottom panels show month versus latitude distributions the amplitude of the quasi-4-day wave (Q4DW) (left) and quasi-6-day wave (Q6DW) (right). The maximum amplitude of the W2 component at periods 3–5 days is taken as the Q4DW amplitude, while the maximum amplitude of the W1 component at periods 4.5–7 days is taken as the Q6DW amplitude. The meridional structures of the (2,1) Rossby normal mode and (1,1) Rossby normal mode are indicated by the white dashed curves. These Hough functions are computed using the code given by Wang et al. (2016). In all panels, the vertical magenta lines correspond to the equinoxes.

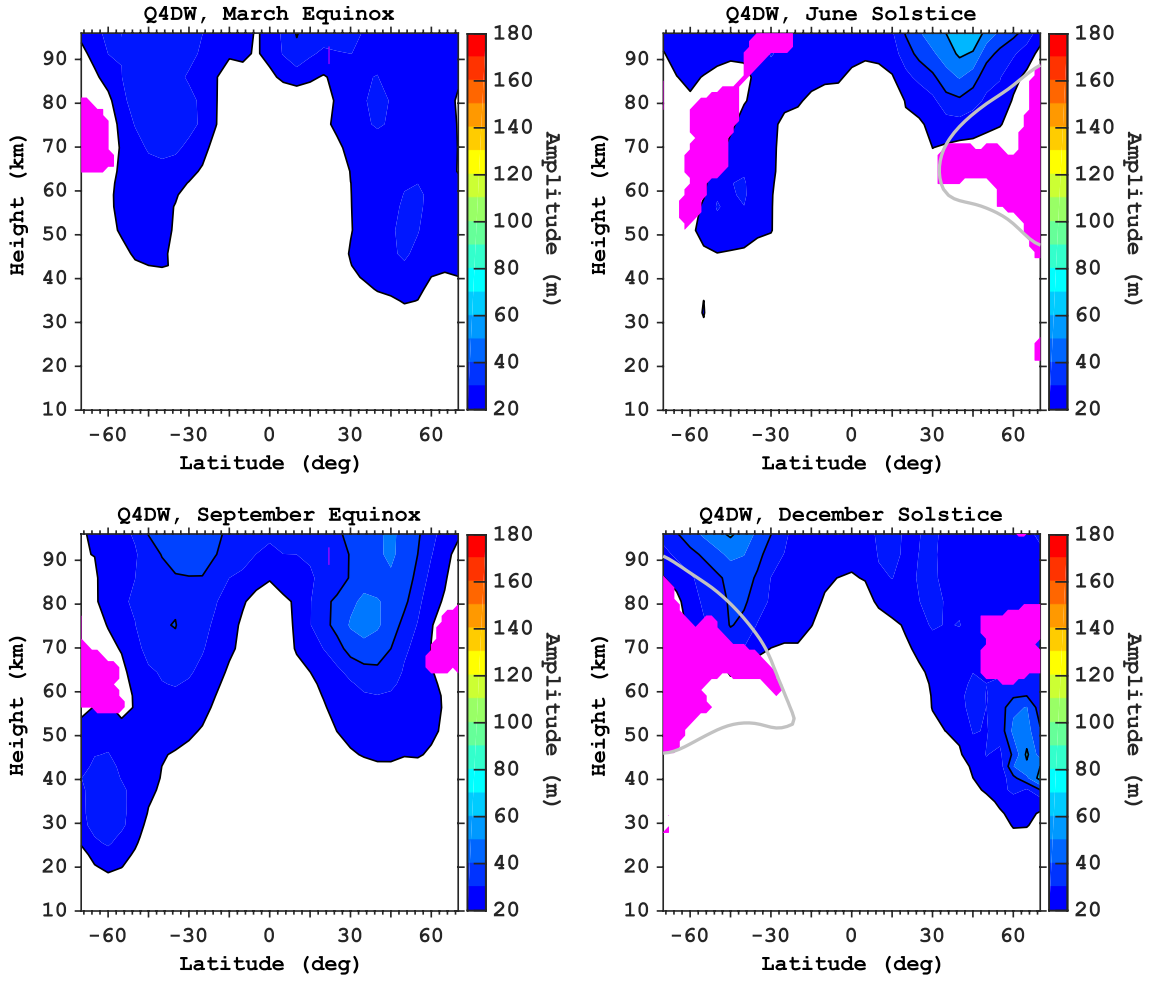

Figure 3. Latitude versus height distributions of the amplitude of the quasi-4-day wave (Q4DW) for 21 March (top left), 21 June (top right), 21 September (bottom left), and 21 December (bottom right). They are climatological representations based on the average of 16 years of the Aura/Microwave Limb Sounder geopotential height observations. The gray lines indicate the boundary of the critical layer for the Q4DW. The magenta shading indicates regions of unstable zonal mean flow ($\overline{q}_y < 0$).

Q4DW presented in Figure 2, unstable regions with $\overline{q}_y < 0$ are confined inside the critical layer and do not extend beyond its boundary. Thus, the wave cannot be amplified or locally excited in the unstable regions.

Figure 4 gives an overview of the Q4DW events in August 16, 2012 and November, 11 2014, where the amplitude was particularly large. The top panels show that the Q4DW, with the amplitude greater than 300 m, was the dominant component of traveling planetary waves in the MLT in both cases. The amplitude structures, presented in the middle panels, are similar to those in the climatological results (Figure 2) but the amplitudes are much larger. The vertical and meridional distributions of the phase are shown in the bottom panels. At altitudes above 50 km or so, downward phase progression with height is seen, indicating upward energy propagation. The vertical wavelength in the MLT, as estimated by fitting a linear regression to the phase values above 60 km, is approximately 58 km at 45°N for the August 2012 event, and 69 km at 45°S for the November 2014 event. These values are comparable with the typical vertical wavelength of the Q6DW, e.g., 60–70 km as reported by Forbes and Zhang (2017). The phase is largely symmetric about the equator, which is consistent with the classical (2,1) mode.

It is noted that there is considerable year-to-year variability in the magnitude of the seasonal enhancement of the Q4DW. This can be seen in Figure 5 for the Northern Hemisphere. Figure 5 shows the amplitude of the Q4DW at 45°N during 2005–2020. Enhanced Q4DW activity is seen in May and August, but the maximum amplitude varies from year to year. We checked distributions of unstable regions ($\overline{q}_y < 0$) and their

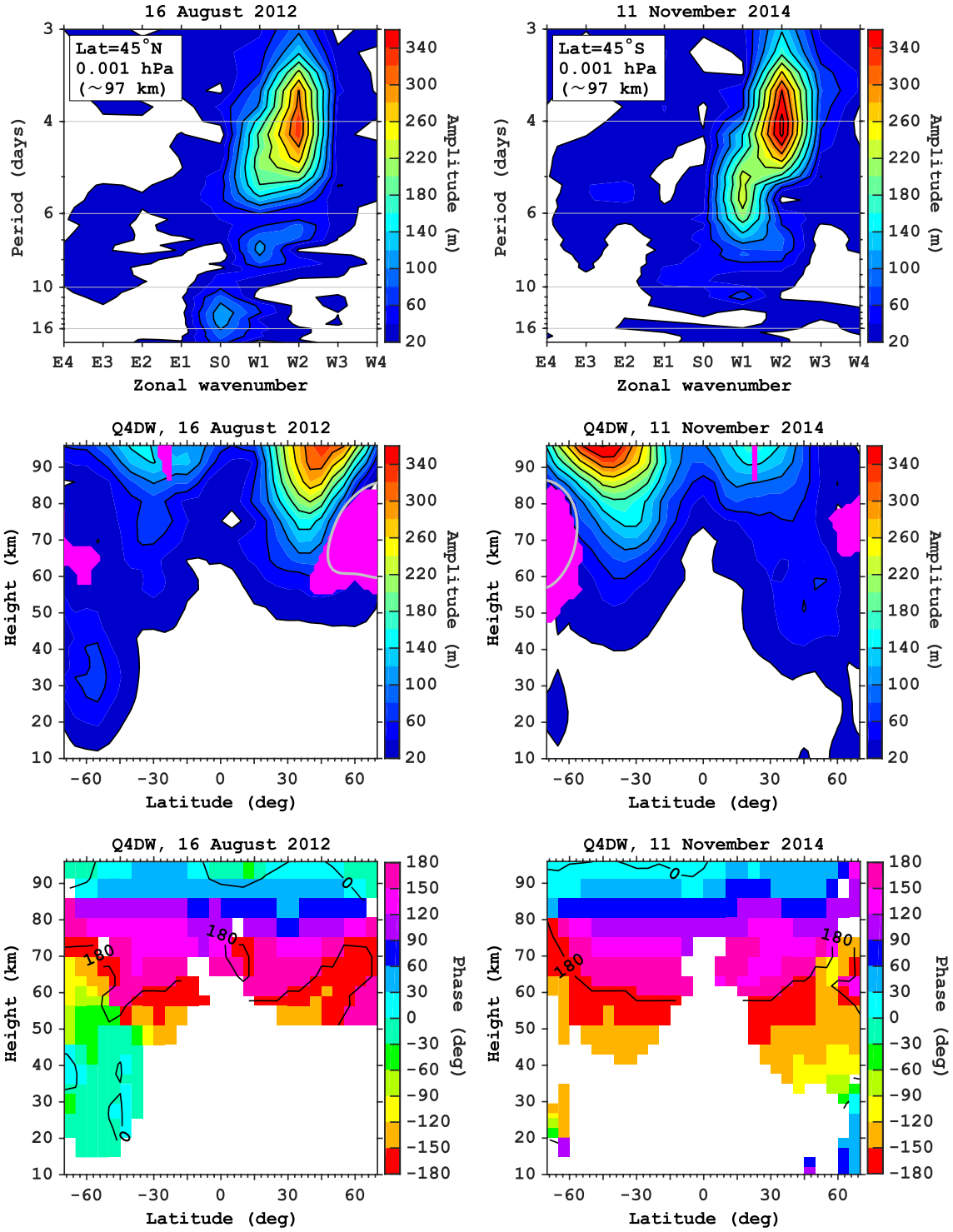

Figure 4. Overview of large-amplitude quasi-4-day wave (Q4DW) events in August 16, 2012 (left) and November 11, 2014 (right). (Top) Zonal wavenumber versus period spectra of Aura/Microwave Limb Sounder geopotential height at 0.001 hPa (97 km). (Middle) Latitude versus height distributions of the Q4DW amplitude. The gray lines indicate the boundary of the critical layer for the Q4DW. The magenta shading indicates regions of unstable zonal mean flow ($\overline{q}_y < 0$). (Bottom) Latitude versus height distributions of the Q4DW phase.

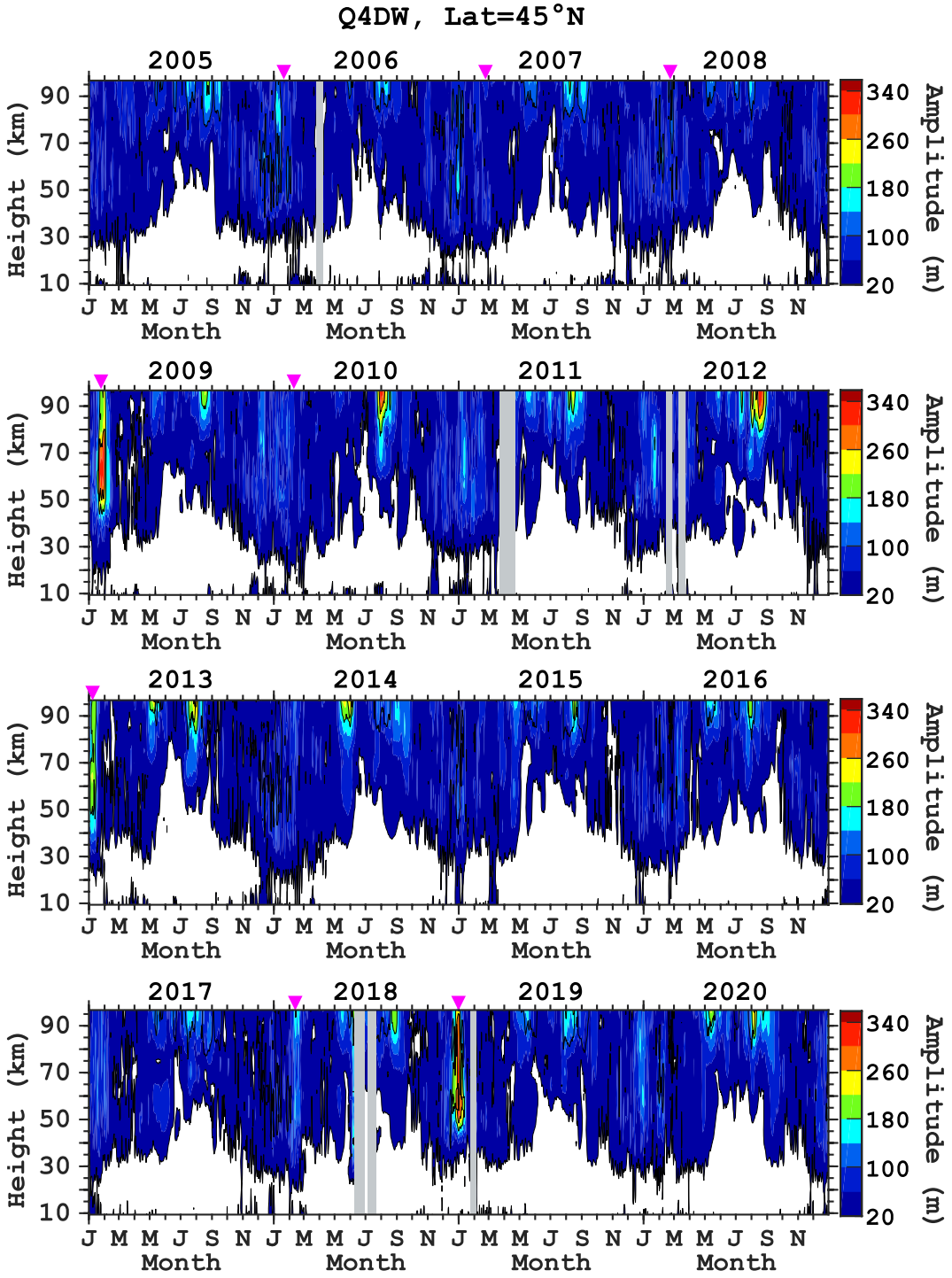

Figure 5. Month versus height plots for the amplitude of the quasi-4-day wave (Q4DW) in Aura/Microwave Limb Sounder (MLS) geopotential height at 45°N from 2005 to 2020. The onset times of the zonal mean zonal wind reversal at 10 hPa (32 km) and 60°N associated with major sudden stratospheric warmings (SSW) are indicated by downward arrows. The identification of the wind reversal is based on Aura/MLS geostrophic winds.

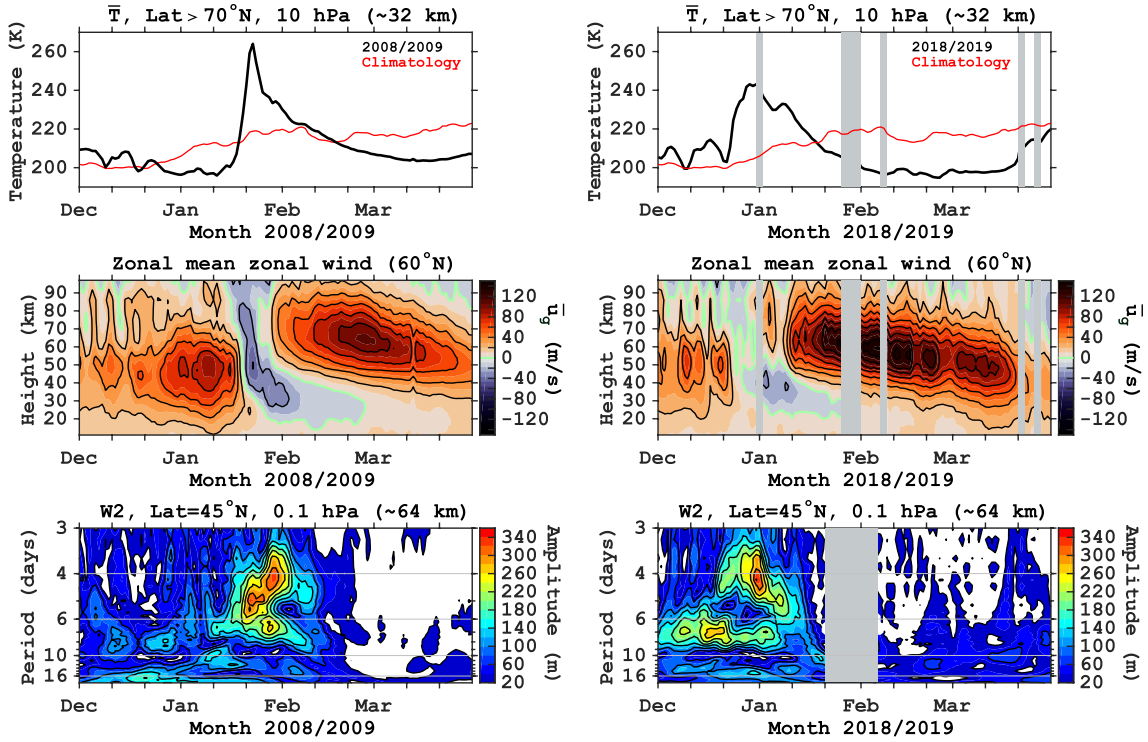

Figure 6. Sudden stratospheric warmings in the boreal winters of 2008/2009 (left) and 2018/2019 (right). The top panels show time series of Aura/Microwave Limb Sounder (MLS) temperature at 10 hPa (32 km) averaged above 70°N (black) and the corresponding climatological seasonal cycle during 2004–2020 (red). The middle panels show month versus height plots of the zonal mean zonal wind at 60°N. The bottom panels show month versus period spectra of Aura/MLS geopotential height at 0.1 hPa (64 km) for the westward-propagating zonal wavenumber 2 (W2) component.

relationship to the critical layer, but did not find a systematic difference in their patterns between the years with relatively large and small seasonal enhancements of the Q4DW. The results suggest that the consideration of the critical layer and atmospheric instability alone is not sufficient to explain the year-to-year variability of the Q4DW. A possible explanation is the propagation of the Q4DW from the lower atmosphere, which could vary from year to year.

3.2. Quasi-4-Day Wave Event During Sudden Stratospheric Warmings

In Figure 5, enhanced wave activity is occasionally seen in the mesosphere during boreal winters. Such an unseasonal enhancement of the Q4DW is not observed in the Southern Hemisphere (not shown here). The bursts of Q4DW activity in the Northern Hemisphere during winter coincide with major SSW, which are also indicated in Figure 5. Examples of such are the SSW in January 2009, January 2013, February 2018, and January 2019. The response is particularly prominent during the January 2009 and January 2019 events. Below we examine the W2 response to SSW in more detail. The response of the W1 component to SSW is presented in Yamazaki and Matthias (2019) and thus will not be considered here.

Figure 6 depicts the W2 response to the SSW in January 2009 and January 2019, when the Q4DW response is most pronounced. A rapid increase in the polar stratospheric temperature (top panels), together with the reversal of the zonal mean zonal wind (middle panels), indicates the occurrence of SSW. The January 2009 event (left panels) is one of the strongest major warmings in the record (e.g., Manney et al., 2009; Harada et al., 2010) and its whole atmosphere impact has been extensively studied (e.g., Jin et al., 2012; Pedatella et al., 2014). According to Aura/MLS geostrophic winds, the reversal of the zonal wind at 32 km and 60°N occurred on 24 January 2009. At 64 km, enhanced wave activity in the W2 component is observed at a period of ~5 days around 22–26 January and ~4 days around 27–31 January. The January 2019 event is another major warming (e.g., Rao et al., 2019) but the middle atmosphere response is not as pronounced as that

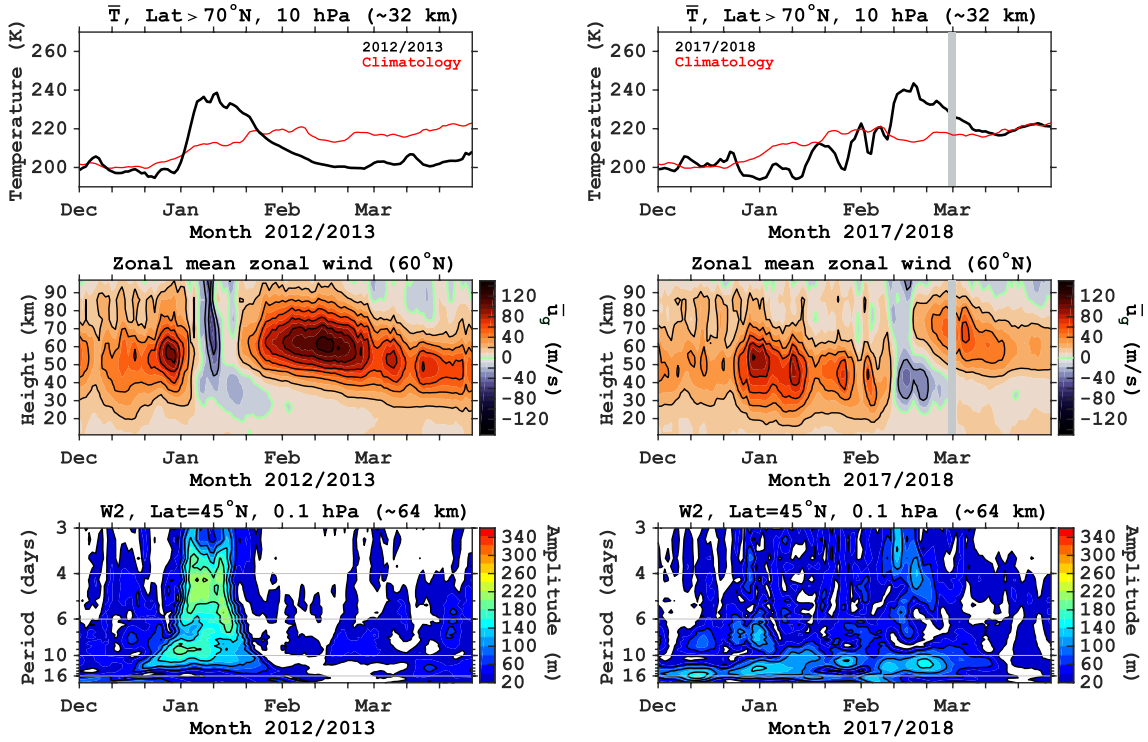

Figure 7. Same as Figure 6 but for sudden stratospheric warmings in the boreal winters of 2012/2013 (left) and 2017/2018 (right).

during the January 2009 event. The wind reversal at 32 km was recorded on 31 December 2018. Strong wave activity is in the W2 component at a period ~4 days around 30 December 2018–2 January 2019.

In Figure 6, enhanced W2 wave activity is also seen at a period of ~7 days during both the SSW, which may be related to the first asymmetric mode of zonal wavenumber 2, or the (2,2) mode. Largest ~7-day oscillations are observed at ~50°N (not shown here), which is consistent with the (2,2) mode. The expected antisymmetric phase structure was, however, not detected, as the waves are mostly confined to the Northern Hemisphere and it was difficult to determine the phase in the Southern Hemisphere.

Figure 7 shows the W2 response to major warming events in January 2013 (left panels) and February 2018 (right panels). For the January 2013 event, the wind reversal at 32 km occurred on 7 January 2013, and enhanced wave activity in the W2 component at periods 4–5 days is observed at 64 km around 5–13 January 2013. For the February 2018 event, the wind reversal took place on 12 February 2018. Although W2 wave activity during this SSW was not as strong as that during the other SSW mentioned above, a minor burst of ~4-day wave activity was observed around 16–20 February 2018.

Figure 8 compares the height structures of the Q4DW before SSW (left panels), during SSW (middle panels) and after SSW (right panels) for the events, from the top to the bottom, in the boreal winters of 2008/2009, 2018/2019, 2012/2013, 2017/2018, and 2005/2006. The central date assigned as "during SSW" is January 30, 2009 for the 2008/2009 event, January 1, 2019 for the 2018/2019 event, January 13, 2013 for the 2012/2013 event, February 13, 2018 for the 2017/2018 event, and January 25, 2006 for the 2005/2006 event. The dates 20 days before and after the central dates are assigned as "before SSW" and "after SSW," respectively.

Before SSW (left panels), the distributions of the critical layer and unstable mean flow are similar to the climatological pattern for the December solstice presented in Figure 3. That is, a critical layer exists in the Southern Hemisphere at mesospheric heights, within which unstable regions with $\overline{q}_y < 0$ are confined. During SSW (middle panels), an additional critical layer appears in the Northern Hemisphere high-latitude region, and a region of unstable mean flow extends beyond the critical layer. The formation of the critical layer and unstable region in the Northern Hemisphere is a direct result of the zonal wind reversal connected to SSW. As discussed earlier in the context of the seasonal amplification of the Q4DW (Figure 2), an

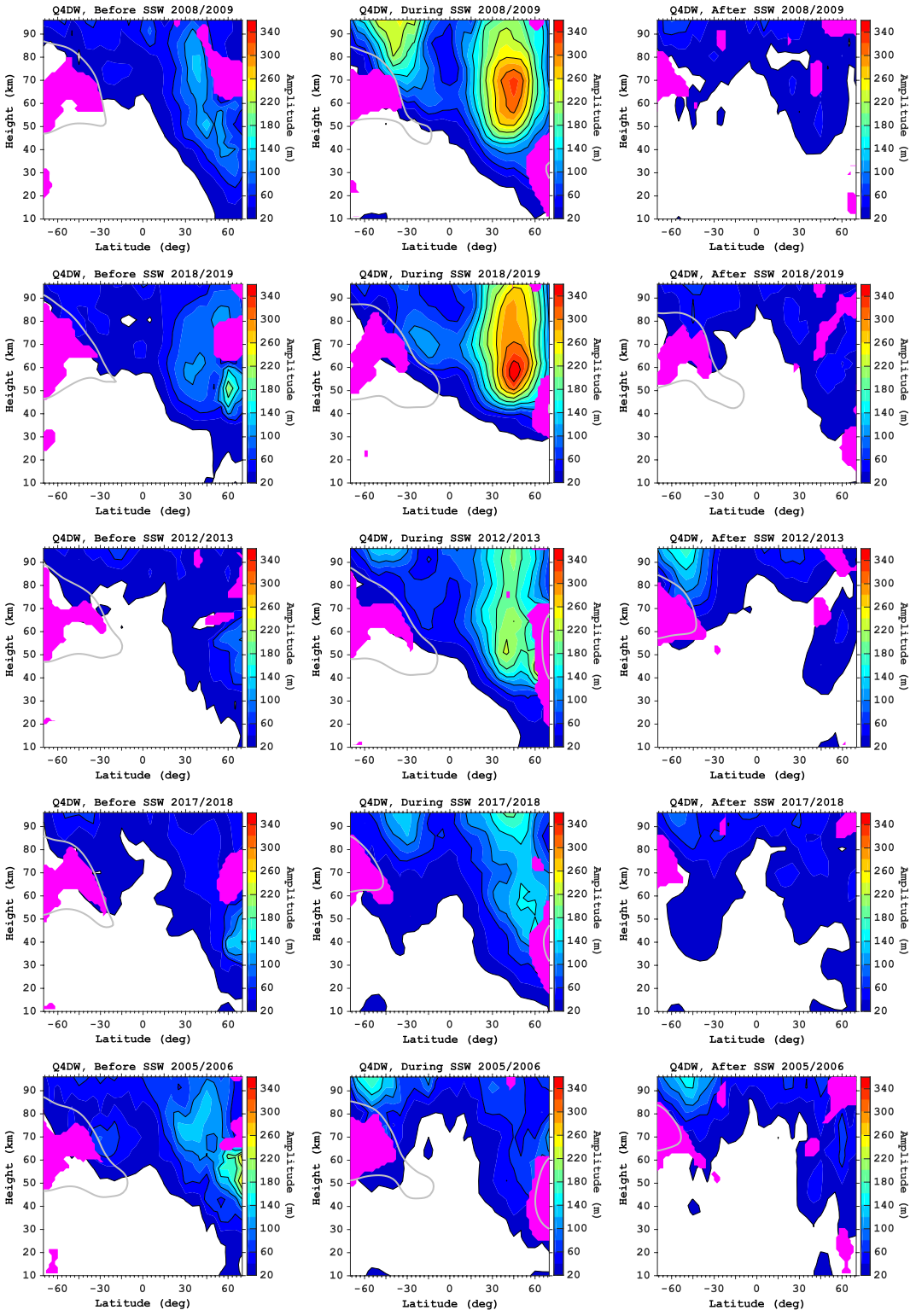

Figure 8. Latitude versus height distributions of the quasi-4-day wave (Q4DW) amplitude during sudden stratospheric warmings in the boreal winters of, from the top to the bottom, 2008/2009, 2018/2019, 2012/2013, 2017/2018, and 2005/2006. The central date for each event is January 30, 2009, January 1, 2019, January 13, 2013, February 13, 2018 and January 25, 2006. For comparisons, the results are also presented for 20 days before (left) and after (right) the central dates. The gray lines indicate the boundary of the critical layer for the Q4DW. The magenta shading indicates regions of unstable zonal mean flow ($\overline{q}_y < 0$).

unstable region extending across the boundary of the critical layer gives a favorable condition for vertical growth of the Q4DW. After SSW (right panels), the state of the background atmosphere is different depending on the event. No critical layer is seen after the January 2009 and February 2018 events, and overall Q4DW activity is low, similar to the equinox cases (Figure 3). After the 2018/2019 event, the background atmosphere went back to the December solstice type, with the critical layer in the Southern Hemisphere encompassing an unstable region, and thus there is no Q4DW enhancement. After the January 2006 and 2013 events, the Q4DW in the Southern Hemisphere MLT is enhanced, as the critical layer moves to higher latitudes and an unstable region extends across the boundary of the critical layer, which represents typical February conditions (Figure 2).

A difference between Q4DW enhancement during SSW and seasonal Q4DW enhancement is that during SSW, the wave amplification occurs at lower heights than during times of seasonal enhancement. This can be understood from the fact that during periods of seasonal enhancement, the critical layer and unstable regions appear in the mesosphere (50–80 km), while they are mainly in the stratosphere (20–50 km) during SSW. Figure 9 shows the vertical growth rate of the Q4DW amplitude during the January 2009 and 2019 SSW (top panels). Largest wave growth is observed at 40–50 km, where the zonal wind relative to the wave is reduced. At MLT altitudes, the zonal wind is strongly eastward relative to the wave, which prevents vertical growth of the wave. During seasonal enhancement of the Q4DW (bottom panels), on the other hand, largest wave growth occurs in the MLT, as the zonal wind is weakly eastward relative to the wave.

The previous study by Ma et al. (2020) reported enhanced Q4DW activity in the MLT during the 2018/2019 SSW. They suspected that the barotropic/baroclinic instability might be the source of the wave. Our results support this possibility. We also put emphasis on the presence of the critical layer, around which the vertical growth rate of quasi-normal modes are predicted to increase (Salby, 1981a). Gu et al. (2018) pointed out that changes in the distributions of the critical layer and unstable regions can explain the response of the quasi-2-day wave (a manifestation of mixed Rossby-gravity wave) to the SSW in January 2006. A similar concept is used here to understand the behavior of the Q4DW during SSW events. Sassi et al. (2012), examining quasi-normal modes in the middle atmosphere during SSW, noted that the Q4DW was present during the January 2009 event but not during other SSW in 2006 and 2008. We have confirmed their findings. Q4DW activity was strong during the SSW in January 2009 and 2019. Enhanced but weaker wave activity was detected during the SSW in January 2013 and February 2018. For other years, it was difficult to identify wave activity associated with the Q4DW, including the major warming in January 2006.

It remains unclear why some SSW are accompanied by stronger Q4DW activity than others. Properties of SSW depend on various factors, including the SSW type, quasi-biennial oscillation (QBO) phase, and solar flux (e.g., Charlton & Polvani, 2007; Camp & Tung, 2007), and accordingly, the wave response to SSW can also vary depending on them (Pogoreltsev et al., 2014; Siddiqui et al., 2018). An SSW can be classified into wave-1 and wave-2 types, which are driven by enhanced planetary wave forcing with zonal wavenumber 1 and 2, respectively. Wave-1 and wave-2 types are generally associated with the displacement and splitting of the polar vortex. Figure 10 shows daily amplitudes of wave-1 and wave-2 components of the planetary wave at 10 hPa (32 km) and 60°N during each SSW, as determined by the Fourier analysis of Aura/MLS geopotential height data (solid line) as well as the corresponding data from the NCEP-DOE Reanalysis 2 (Kanamitsu et al., 2002) (dashed line). Choi et al. (2019) introduced a simple method to distinguish between wave-1 and wave-2 types. That is, if the wave-2 amplitude exceeds the wave-1 amplitude on any day during ±10 days from the reversal of the zonal mean zonal wind, the event is said to be wave-2 type; otherwise, it is called wave-1 type. Based on this definition, the February 2007, January 2009, January 2013, and February 2018 SSW are wave-2 type and the rest is wave-1 type. Although the January 2019 event is classified here as wave-1 type, Rao et al. (2019) pointed out that this SSW was neither typical wave-1 nor wave-2 type, involving complex forcing from waves 1–3 following the SSW onset. They observed split of the polar vortex in synoptic charts of the 10-hPa heights starting around 4–8 January 2019. This is after peak activity of the Q4DW, and thus the vortex split during the January 2019 SSW is unlikely involved in the Q4DW enhancement. The vertical green lines in Figure 10 indicate the central date of Q4DW events. In summary, there is no apparent correlation between the occurrence of Q4DW enhancement during SSW and the type of the SSW. Also, Q4DW enhancement during SSW is observed under both easterly and westerly phases of the QBO, regardless of the solar flux level. The QBO phase, determined by the equatorial zonal mean zonal wind at

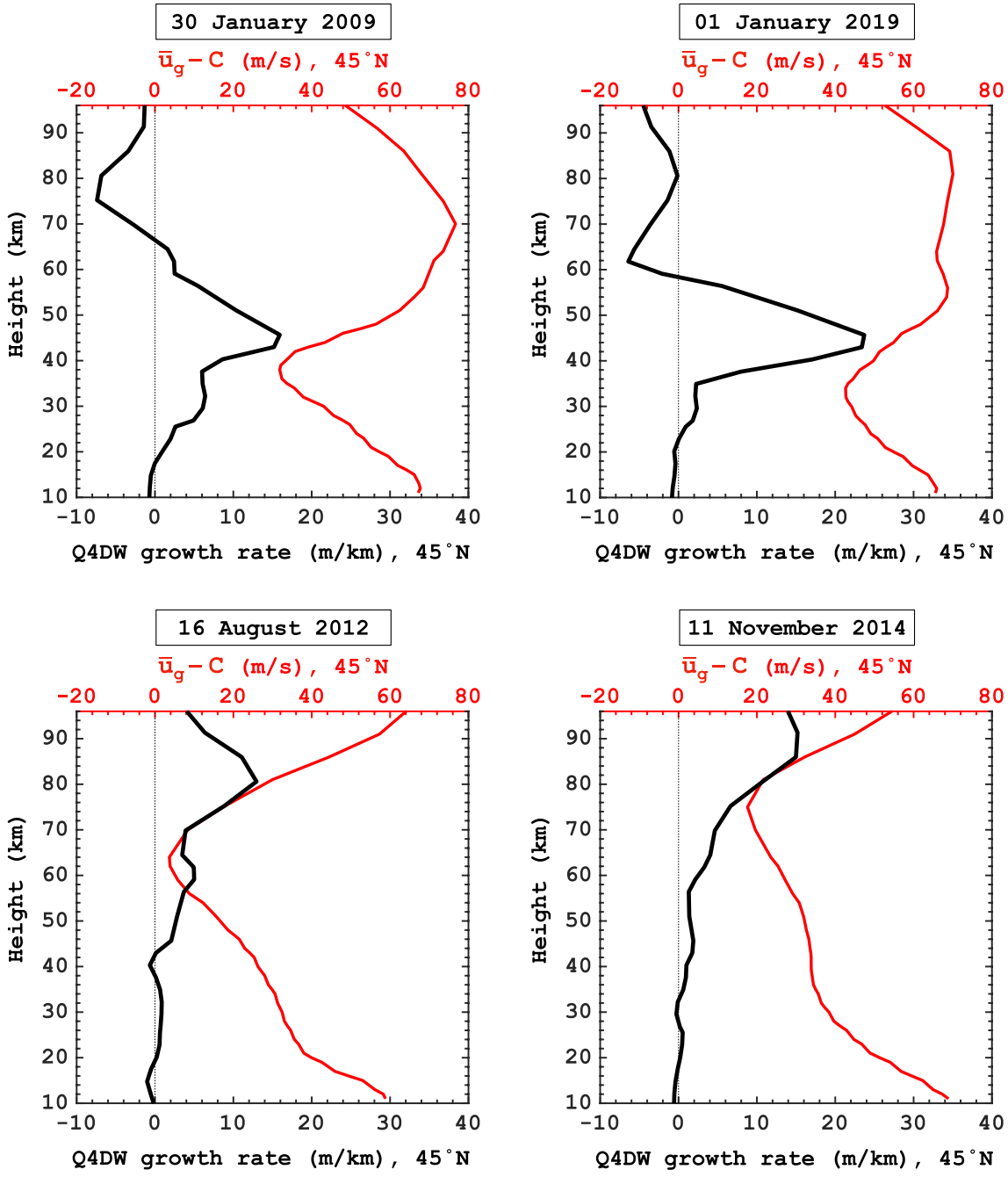

Figure 9. Vertical growth rate of the quasi-4-day wave (Q4DW) at 45°N for January 30, 2009 (upper left), January 1, 2019 (upper right), August 16, 2012 (lower left) and November 11, 2014 (lower right). The red curves indicate the zonal mean zonal wind velocity at 45°N relative to the phase speed of the Q4DW.

50 hPa from the NCEP-DOE Reanalysis 2, is indicated in Figure 10 for each SSW, along with the solar flux index $F_{10.7}$ (Tapping, 2013).

4. Summary and Conclusions

Aura/MLS geopotential height data have been used to examine the westward-propagating ~4-day wave with zonal wavenumber 2, or quasi-4-day wave (Q4DW), in the middle atmosphere, which is regarded as a manifestation of the (2,1) Rossby normal mode in the presence of dissipation and nonuniform background.

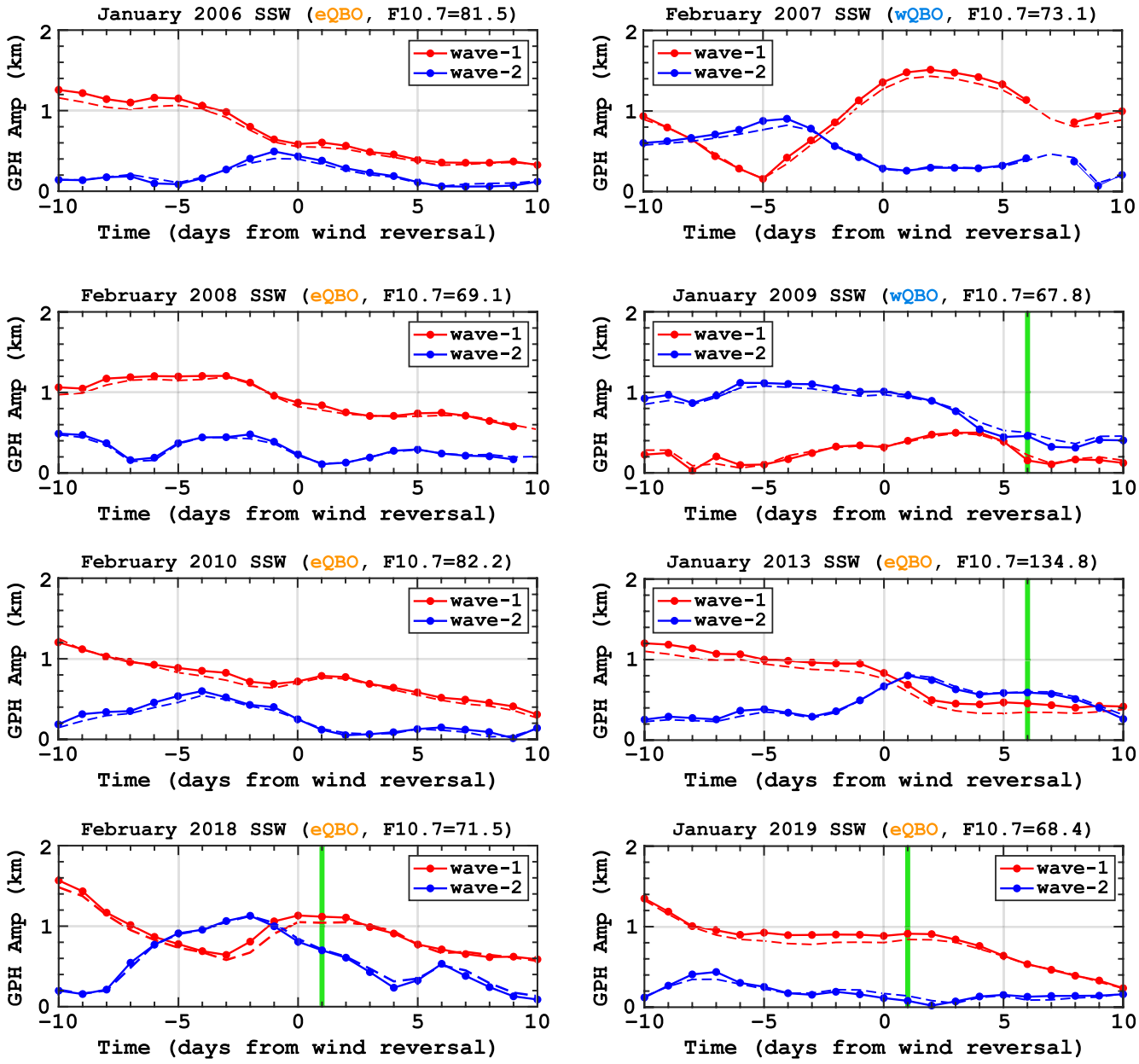

Figure 10. Overview of major sudden stratospheric warmings observed during 2005–2020. Red and blue lines show daily amplitudes of wave-1 and wave-2 planetary waves at 60°N at 10 hPa, respectively. Solid lines correspond to amplitudes derived from Aura/MLS geopotential height (GPH) data, while dashed lines are the same but from the NCEP-DOE Reanalysis 2. Vertical green lines indicate the central date of quasi-4-day wave enhancement. Phase of the quasi-biennial oscillation (QBO) is indicated for each SSW. eQBO and wQBO correspond to easterly and westerly phases of the QBO, respectively, which are determined by the equatorial zonal wind at 50 hPa from the NCEP-DOE Reanalysis 2 averaged over ±10 days from the day of the zonal wind reversal at 60°N at 10 hPa. The solar flux index $F_{10.7}$ averaged over the same time interval is also indicated for each SSW. The dates of wind reversal are January 21, 2006, February 22, 2007, February 22, 2008, January 24, 2009, February 8, 2010, January 7, 2013, February 12, 2018, and December 31, 2018.

The seasonal climatology of the Q4DW is obtained from the data during August 2004–December 2020. The main results may be summarized as follows:

1. Geopotential height perturbations of the Q4DW in the mesosphere and lower thermosphere (MLT) are largest at middle latitudes, approximately ±45° latitudes, reflecting the meridional structure of the classical (2,1) mode.

2. Seasonal amplification of the Q4DW in the MLT occurs in May and August in the Northern Hemisphere, and in February and November in the Southern Hemisphere. The mean period of the Q4DW is 3.8 ± 0.4 days.
3. The Q4DW amplitude is generally smaller than that of the quasi-6-day wave (Q6DW), which is a manifestation of the (1,1) Rossby normal mode. Nevertheless, the Q4DW occasionally becomes the predominant component of traveling planetary waves in the MLT with the geopotential height amplitude exceeding 300 m.
4. The phase is symmetric about the equator, which is consistent with the (2,1) mode. At MLT altitudes, the vertical structure of the phase shows downward progression with height, with the vertical wavelength of approximately 60–70 km. The downward phase propagation is consistent with the quasi-normal mode behavior under the presence of dissipation and nonuniform background fields.
5. The seasonal variation of the Q4DW in the MLT can be explained in terms of background conditions. During the seasonal enhancement of the Q4DW, the vertical growth of the wave is increased near the critical layer as predicted by the modeling work by Salby (1981a). At the same time, an unstable region ($\overline{q}_y < 0$) extends across the boundary of the critical layer, where the wave can be amplified or locally excited by extracting energy from the unstable mean flow.
6. During the equinoxes, the Q4DW amplitude in the MLT is small, as there is no critical layer. During the solstices, the critical layer exists in the summer hemisphere, but the Q4DW amplitude is not as large as that during May, August, February and November, as unstable regions with $\overline{q}_y < 0$ are confined within the critical layer.
7. In addition to the seasonal amplification, the Q4DW sometimes attains a large amplitude in the MLT during times of Arctic sudden stratospheric warmings (SSW). This can be explained by the distributions of the critical layer and unstable mean flow, in a similar way as the seasonal amplification. Q4DW enhancement is observed during both wave-1 and wave-2 types of SSW, regardless of the quasi-biennial oscillation phase and solar flux level.

This study has established that the Q4DW is an important part of atmospheric variability at MLT heights. The seasonal amplification of the Q4DW is a robust feature, but the extent of the amplification varies from year to year. Similarly, the extent of the Q4DW amplification during SSW also varies from event to event. More studies are needed to understand the mechanism for these variabilities. Also, a broader impact of the Q4DW on the ionosphere/thermosphere system still needs to be assessed in future work.

Data Availability Statement

We thank the NASA Goddard Earth Sciences (GES) Data and Information Services Center (DISC) (https://disc.gsfc.nasa.gov/) for making the Aura/MLS geopotential height data (https://doi.org/10.5067/Aura/MLS/DATA2008) available.

Acknowledgments
This work was supported in part by JSPS and DFG (grant YA-574-3-1) under the Joint Research Projects-LEAD with DFG. Open access funding enabled and organized by Projekt DEAL.

References

Allen, D., Stanford, J., Elson, L., Fishbein, E., Froidevaux, L., & Waters, J. (1997). The 4-day wave as observed from the upper atmosphere research satellite microwave limb sounder. *Journal of the Atmospheric Sciences*, *54*(3), 420–434. https://doi.org/10.1175/1520-0469(1997)054<0420:tdwaof>2.0.co;2

Andrews, D. G., Leovy, C. B., & Holton, J. R. (1987). Middle Atmosphere Dynamics (Vol. 40). Academic press.

Camp, C. D., & Tung, K.-K. (2007). The influence of the solar cycle and qbo on the late-winter stratospheric polar vortex. *Journal of the Atmospheric Sciences*, *64*(4), 1267–1283. https://doi.org/10.1175/jas3883.1

Charlton, A. J., & Polvani, L. M. (2007). A new look at stratospheric sudden warmings. Part I: Climatology and modeling benchmarks. *Journal of Climate*, *20*(3), 449–469. https://doi.org/10.1175/jcli3996.1

Choi, H., Kim, B.-M., & Choi, W. (2019). Type classification of sudden stratospheric warming based on pre-and postwarming periods. *Journal of Climate*, *32*(8), 2349–2367. https://doi.org/10.1175/jcli-d-18-0223.1

Day, K., & Mitchell, N. (2010). The 16-day wave in the arctic and antarctic mesosphere and lower thermosphere. *Atmospheric Chemistry and Physics*, *10*(3), 1461–1472. https://doi.org/10.5194/acp-10-1461-2010

Forbes, J. M. (1995). Tidal and planetary waves. *The Upper Mesosphere and Lower Thermosphere: A Review of Experiment and Theory. Geophysical Monograph Series*, 87, 67–87.

Forbes, J. M., & Zhang, X. (2015). Quasi-10-day wave in the atmosphere. *Journal of Geophysical Research: Atmospheres*, *120*(21), 11–079. https://doi.org/10.1002/2015jd023327

Forbes, J. M., & Zhang, X. (2017). The quasi-6 day wave and its interactions with solar tides. *Journal of Geophysical Research: Space Physics*, *122*(4), 4764–4776. https://doi.org/10.1002/2017ja023954

Gan, Q., Oberheide, J., & Pedatella, N. M. (2018). Sources, sinks, and propagation characteristics of the quasi 6-day wave and its impact on the residual mean circulation. *Journal of Geophysical Research: Atmospheres*, *123*(17), 9152–9170. https://doi.org/10.1029/2018jd028553

Gan, Q., Oberheide, J., Yue, J., & Wang, W. (2017). Short-term variability in the ionosphere due to the nonlinear interaction between the 6 day wave and migrating tides. *Journal of Geophysical Research: Space Physics*, *122*(8), 8831–8846. https://doi.org/10.1002/2017ja023947

Gu, S.-Y., Dou, X., Pancheva, D., Yi, W., & Chen, T. (2018). Investigation of the abnormal quasi 2-day wave activities during the sudden stratospheric warming period of January 2006. *Journal of Geophysical Research: Space Physics*, *123*(7), 6031–6041. https://doi.org/10.1029/2018ja025596

Gu, S.-Y., Liu, H.-L., Li, T., Dou, X., Wu, Q., & Russell, J. M. (2014). Observation of the neutral-ion coupling through 6 day planetary wave. *Journal of Geophysical Research: Space Physics*, *119*(12), 10–376. https://doi.org/10.1002/2014ja020530

Harada, Y., Goto, A., Hasegawa, H., Fujikawa, N., Naoe, H., & Hirooka, T. (2010). A major stratospheric sudden warming event in January 2009. *Journal of the Atmospheric Sciences*, *67*(6), 2052–2069. https://doi.org/10.1175/2009jas3320.1

He, M., Yamazaki, Y., Hoffmann, P., Hall, C. M., Tsutsumi, M., Li, G., & Chau, J. L. (2020). Zonal wave number diagnosis of Rossby wave-like oscillations using paired ground-based radars. *Journal of Geophysical Research: Atmospheres*, *125*(12), e2019JD031599. https://doi.org/10.1029/2019jd031599

Hirooka, T. (2000). Normal mode Rossby waves as revealed by UARS/ISAMS observations. *Journal of the Atmospheric Sciences*, *57*(9), 1277–1285. https://doi.org/10.1175/1520-0469(2000)057<1277:nmrwar>2.0.co;2

Hirooka, T., & Hirota, I. (1985). Normal mode Rossby waves observed in the upper stratosphere. Part II: Second antisymmetric and symmetric modes of zonal wavenumbers 1 and 2. *Journal of the Atmospheric Sciences*, *42*(6), 536–548. https://doi.org/10.1175/1520-0469(1985)042<0536:nmrwoi>2.0.co;2

Hirota, I., & Hirooka, T. (1984). Normal mode Rossby waves observed in the upper stratosphere. Part I: First symmetric modes of zonal wavenumbers 1 and 2. *Journal of the Atmospheric Sciences*, *41*(8), 1253–1267. https://doi.org/10.1175/1520-0469(1984)041<1253:nmrwoi>2.0.co;2

Jin, H., Miyoshi, Y., Pancheva, D., Mukhtarov, P., Fujiwara, H., & Shinagawa, H. (2012). Response of migrating tides to the stratospheric sudden warming in 2009 and their effects on the ionosphere studied by a whole atmosphere-ionosphere model GAIA with COSMIC and TIMED/SABER observations. *Journal of Geophysical Research: Space Physics*, *117*(A10). https://doi.org/10.1029/2012ja017650

Kanamitsu, M., Ebisuzaki, W., Woollen, J., Yang, S.-K., Hnilo, J., Fiorino, M., & Potter, G. (2002). NCEP–DOE AMIP-II Reanalysis (R-2). *Bulletin of the American Meteorological Society*, *83*(11), 1631–1643. https://doi.org/10.1175/bams-83-11-1631(2002)083<1631:nar>2.3.co;2

Kasahara, A. (1976). Normal modes of ultralong waves in the atmosphere. *Monthly Weather Review*, *104*(6), 669–690. https://doi.org/10.1175/1520-0493(1976)104<0669:nmouwi>2.0.co;2

Kasahara, A. (1980). Effect of zonal flows on the free oscillations of a barotropic atmosphere. *Journal of the Atmospheric Sciences*, *37*(5), 917–929. https://doi.org/10.1175/1520-0469(1980)037<0917:eozfot>2.0.co;2

Labitzke, K., & Loon, Van, H. (1999). *The stratosphere: Phenomena, history, and relevance*. Springer Science & Business Media.

Lieberman, R., Riggin, D., Franke, S., Manson, A., Meek, C., Nakamura, T., & Reid, I. (2003). The 6.5-day wave in the mesosphere and lower thermosphere: Evidence for baroclinic/barotropic instability. *Journal of Geophysical Research: Atmospheres*, *108*(D20). https://doi.org/10.1029/2002jd003349

Lindzen, R. S., & Chapman, S. (1969). Atmospheric tides. *Space Science Reviews*, *10*(1), 3–188. https://doi.org/10.1007/bf00171584

Liu, H.-L., Talaat, E., Roble, R., Lieberman, R., Riggin, D., & Yee, J.-H. (2004). The 6.5-day wave and its seasonal variability in the middle and upper atmosphere. *Journal of Geophysical Research: Atmospheres*, *109*(D21). https://doi.org/10.1029/2004jd004795

Lu, X., Chu, X., Fuller-Rowell, T., Chang, L., Fong, W., & Yu, Z. (2013). Eastward propagating planetary waves with periods of 1–5 days in the winter antarctic stratosphere as revealed by MERRA and lidar. *Journal of Geophysical Research: Atmospheres*, *118*(17), 9565–9578. https://doi.org/10.1002/jgrd.50717

Ma, Z., Gong, Y., Zhang, S., Zhou, Q., Huang, C., Huang, K., & Li, G. (2020). Study of a Quasi 4-day oscillation during the 2018/2019 SSW over Mohe, China. *Journal of Geophysical Research: Space Physics*, *125*(7), e2019JA027687. https://doi.org/10.1029/2019ja027687

Madden, R. A. (1979). Observations of large-scale traveling Rossby waves. *Reviews of Geophysics*, *17*(8), 1935–1949.

Madden, R. A. (2007). Large-scale, free Rossby waves in the atmosphere—An update. *Tellus A: Dynamic Meteorology and Oceanography*, *59*(5), 571–590. https://doi.org/10.1111/j.1600-0870.2007.00257.x

Manney, G. L., Schwartz, M. J., Krüger, K., Santee, M. L., Pawson, S., Lee, J. N., & Livesey, N. J. (2009). Aura microwave limb sounder observations of dynamics and transport during the record-breaking 2009 arctic stratospheric major warming. *Geophysical Research Letters*, *36*(12). https://doi.org/10.1029/2009gl038586

Matthias, V., & Ern, M. (2018). On the origin of the mesospheric quasi-stationary planetary waves in the unusual arctic winter 2015/2016. *Atmospheric Chemistry and Physics*, *18*(7), 4803–4815. https://doi.org/10.5194/acp-18-4803-2018

Matthias, V., Hoffmann, P., Rapp, M., & Baumgarten, G. (2012). Composite analysis of the temporal development of waves in the polar MLT region during stratospheric warmings. *Journal of Atmospheric and Solar-Terrestrial Physics*, *90*, 86–96. https://doi.org/10.1016/j.jastp.2012.04.004

McDonald, A., Hibbins, R. E., & Jarvis, M. J. (2011). Properties of the quasi 16 day wave derived from EOS MLS observations. *Journal of Geophysical Research: Atmospheres*, *116*(D6). https://doi.org/10.1029/2010jd014719

Meek, C., & Manson, A. (2009). Summer planetary-scale oscillations: Aura mls temperature compared with ground-based radar wind. *Annales Geophysicae*, *27*, 1763–1774. https://doi.org/10.5194/angeo-27-1763-2009

Meyer, C. K., & Forbes, J. M. (1997). A 6.5-day westward propagating planetary wave: Origin and characteristics. *Journal of Geophysical Research: Atmospheres*, *102*(D22), 26173–26178. https://doi.org/10.1029/97jd01464

Miyoshi, Y., & Hirooka, T. (1999). A numerical experiment of excitation of the 5-day wave by a GCM. *Journal of the Atmospheric Sciences*, *56*(11), 1698–1707. https://doi.org/10.1175/1520-0469(1999)056<1698:aneoeo>2.0.co;2

Miyoshi, Y., & Yamazaki, Y. (2020). Excitation mechanism of ionospheric 6-day oscillation during the 2019 september sudden stratospheric warming event. *Journal of Geophysical Research: Space Physics*, *125*(9), e2020JA028283. https://doi.org/10.1029/2020ja028283

Pancheva, D., Mukhtarov, P., Mitchell, N., Merzlyakov, E., Smith, A., Andonov, et al. (2008). Planetary waves in coupling the stratosphere and mesosphere during the major stratospheric warming in 2003/2004. *Journal of Geophysical Research: Atmospheres*, *113*(D12). https://doi.org/10.1029/2007jd009011

Pedatella, N., Fuller-Rowell, T., Wang, H., Jin, H., Miyoshi, Y., Fujiwara, H., et al. (2014). The neutral dynamics during the 2009 sudden stratosphere warming simulated by different whole atmosphere models. *Journal of Geophysical Research: Space Physics*, *119*(2), 1306–1324. https://doi.org/10.1002/2013ja019421

Pogoreltsev, A., Savenkova, E., & Pertsev, N. (2014). Sudden stratospheric warmings: The role of normal atmospheric modes. *Geomagnetism and Aeronomy*, *54*(3), 357–372. https://doi.org/10.1134/s0016793214020169

Qin, Y., Gu, S.-Y., Teng, C.-K.-M., Dou, X.-K., Yu, Y., & Li, N. (2021). Comprehensive study of the climatology of the quasi-6-day wave in the MLT region based on aura/MLS observations and SD-WACCM-X simulations. *Journal of Geophysical Research: Space Physics*, *126*(1), e28454. https://doi.org/10.1029/2020JA028454

Randel, W. J., & Lait, L. R. (1991). Dynamics of the 4-day wave in the southern hemisphere polar stratosphere. *Journal of the Atmospheric Sciences*, *48*(23), 2496–2508. https://doi.org/10.1175/1520-0469(1991)048<2496:dotdwi>2.0.co;2

Rao, J., Garfinkel, C. I., Chen, H., & White, I. P. (2019). The 2019 new year stratospheric sudden warming and its real-time predictions in multiple S2S models. *Journal of Geophysical Research: Atmospheres*, *124*(21), 11155–11174. https://doi.org/10.1029/2019jd030826

Riggin, D. M., Liu, H.-L., Lieberman, R. S., Roble, R. G., Russell, J. M., Mertens, C. J., et al. (2006). Observations of the 5-day wave in the mesosphere and lower thermosphere. *Journal of Atmospheric and Solar-Terrestrial Physics*, *68*(3–5), 323–339. https://doi.org/10.1016/j.jastp.2005.05.010

Sakazaki, T., & Hamilton, K. (2020). An array of ringing global free modes discovered in tropical surface pressure data. *Journal of the Atmospheric Sciences*, *77*(7), 2519–2539. https://doi.org/10.1175/jas-d-20-0053.1

Salby, M. L. (1981a). Rossby normal modes in nonuniform background configurations. Part 1: Simple fields. *Journal of the Atmospheric Sciences*, *38*(9), 1803–1826. https://doi.org/10.1175/1520-0469(1981)038<1803:rnminb>2.0.co;2

Salby, M. L. (1981b). Rossby normal modes in nonuniform background configurations. Part 2: Equinox and solstice conditions. *Journal of the Atmospheric Sciences*, *38*(9), 1827–1840. https://doi.org/10.1175/1520-0469(1981)038<1827:rnminb>2.0.co;2

Salby, M. L. (1984). Survey of planetary-scale traveling waves: The state of theory and observations. *Reviews of Geophysics*, *22*(2), 209–236. https://doi.org/10.1029/rg022i002p00209

Salby, M. L., & Roper, R. (1980). Long-period oscillations in the meteor region. *Journal of the Atmospheric Sciences*, *37*(1), 237–244. https://doi.org/10.1175/1520-0469(1980)037<0237:lpoitm>2.0.co;2

Sassi, F., Garcia, R., & Hoppel, K. (2012). Large-scale Rossby normal modes during some recent northern hemisphere winters. *Journal of the Atmospheric Sciences*, *69*(3), 820–839. https://doi.org/10.1175/jas-d-11-0103.1

Schwartz, M., Lambert, A., Manney, G., Read, W., Livesey, N., Froidevaux, L., et al. (2008). Validation of the aura microwave limb sounder temperature and geopotential height measurements. *Journal of Geophysical Research: Atmospheres*, *113*(D15). D15S11. https://doi.org/10.1029/2007JD008783

Siddiqui, T. A., Yamazaki, Y., Stolle, C., Lühr, H., Matzka, J., Maute, A., & Pedatella, N. (2018). Dependence of lunar tide of the equatorial electrojet on the wintertime polar vortex, solar flux, and QBO. *Geophysical Research Letters*, *45*(9), 3801–3810. https://doi.org/10.1029/2018gl077510

Tapping, K. (2013). The 10.7 cm solar radio flux ($F_{10.7}$). *Space Weather*, *11*(7), 394–406. https://doi.org/10.1002/swe.20064

Wang, H., Boyd, J. P., & Akmaev, R. A. (2016). On computation of hough functions. *Geoscientific Model Development*, *9*(4), 1477–1488. https://doi.org/10.5194/gmd-9-1477-2016

Waters, J. W., Froidevaux, L., Harwood, R. S., Jarnot, R. F., Pickett, H. M., Read, W. G., et al. (2006). The earth observing system microwave limb sounder (EOS MLS) on the aura satellite. *IEEE Transactions on Geoscience and Remote Sensing*, *44*(5), 1075–1092.

Wu, D., Hays, P., & Skinner, W. (1994). Observations of the 5-day wave in the mesosphere and lower thermosphere. *Geophysical Research Letters*, *21*(24), 2733–2736. https://doi.org/10.1029/94gl02660

Yamazaki, Y., & Matthias, V. (2019). Large-amplitude quasi-10-day waves in the middle atmosphere during final warmings. *Journal of Geophysical Research: Atmospheres*, *124*(17–18), 9874–9892. https://doi.org/10.1029/2019jd030634

Yamazaki, Y., Matthias, V., Miyoshi, Y., Stolle, C., Siddiqui, T., Kervalishvili, G., et al. (2020). September 2019 Antarctic sudden stratospheric warming: Quasi-6-day wave burst and ionospheric effects. *Geophysical Research Letters*, *47*(1), e2019GL086577. https://doi.org/10.1029/2019gl086577

Yamazaki, Y., Stolle, C., Matzka, J., & Alken, P. (2018). Quasi-6-day wave modulation of the equatorial electrojet. *Journal of Geophysical Research: Space Physics*, *123*(5), 4094–4109. https://doi.org/10.1029/2018ja025365

Yu, F. R., Huang, K. M., Zhang, S. D., Huang, C. M., Yi, F., Gong, Y., et al. (2019). Quasi 10-and 16-day wave activities observed through meteor radar and MST radar during stratospheric final warming in 2015 spring. *Journal of Geophysical Research: Atmospheres*, *124*(12), 6040–6056. https://doi.org/10.1029/2019jd030630

Zhao, Y., Taylor, M. J., Pautet, P.-D., Moffat-Griffin, T., Hervig, M. E., Murphy, D. J., et al. (2019). Investigating an unusually large 28-day oscillation in mesospheric temperature over antarctica using ground-based and satellite measurements. *Journal of Geophysical Research: Atmospheres*, *124*(15), 8576–8593. https://doi.org/10.1029/2019jd030286